Baseline Lamina Cribrosa Curvature and Subsequent Visual Field Progression Rate in Primary Open-Angle Glaucoma

Ahnul Ha, MD,[1,2] Tai Jun Kim, MD,[1,2] Michael J.A. Girard, PhD,[3,4] Jean Martial Mari, PhD,[5]
Young Kook Kim, MD,[1,2] Ki Ho Park, MD, PhD,[1,2] Jin Wook Jeoung, MD, PhD[1,2]

Purpose: To investigate the relationship between the degree of posterior bowing of the lamina cribrosa (LC) at baseline and the rate of subsequent visual field (VF) progression in eyes with primary open-angle glaucoma (POAG).

Design: Prospective, observational study.

Participants: One hundred one early-stage (VF mean deviation [MD], −5.0 to −0.01 dB) POAG eyes that met the following conditions: (1) follow-up longer than 3.5 years, (2) more than 5 reliable standard automated perimetry tests, and (3) medically well-controlled intraocular pressure during follow-up.

Methods: All participants underwent swept-source OCT scanning of the LC at baseline. The area enclosed by a vertical line at the anterior laminar insertion, anterior LC plane, and reference plane of Bruch's membrane opening (BMO) was divided by D (distance between the 2 cross-points made by vertical lines drawn from the anterior laminar insertion to the reference plane of BMO) to approximate the LC depth (LCD). The difference between the LCD and mean anterior laminar insertion depth was defined as the LC curvature index (LCCI). To consider the steepness of the LC curve, the adjusted LCCI (aLCCI) was calculated as LCCI divided by D and multiplied by 100. The mean LCD (mLCD), mean LCCI (mLCCI), and mean aLCCI (maLCCI) were computed by averaging the measurements on 12 radial scans. The subsequent MD slope and associated factors were analyzed.

Main Outcome Measures: Lamina cribrosa parameters and subsequent MD slope.

Results: The participants' mean baseline MD was −3.8 ± 3.4 dB. The mean baseline mLCD, mLCCI, and maLCCI were 419.0 ± 111.2 μm, 76.4 ± 29.0 μm, and 4.8 ± 1.9, respectively. A greater MD slope was associated with a greater baseline maLCCI ($P < 0.001$). We found a statistically significant breakpoint for the maLCCI (4.12) above which a larger maLCCI showed a steeper MD slope ($P < 0.001$). Analysis by age revealed that significantly more VF progression with maLCCI changes occurred in the relatively younger group (≤69 years; $P = 0.043$).

Conclusions: The baseline maLCCI showed a significant correlation with the rate of subsequent VF deterioration. This suggests that, in POAG eyes with greater posterior bowing of the LC, the axons of retinal ganglion cells may be more vulnerable to further glaucomatous injury. *Ophthalmology 2018;125:1898-1906 © 2018 by the American Academy of Ophthalmology*

It is well established that the primary site of pathogenesis in glaucoma is the lamina cribrosa (LC).[1–6] Biomechanical changes to the LC induce retinal ganglion cell (RGC) axonal injury, eventually causing glaucomatous optic neuropathy.[3–6] The role of LC deformation in RGC death has been attributed to both mechanical and ischemic causes. Lamina cribrosa compression and backward bowing can incur kinking and pinching of axons directly in laminar pores, thus blocking, or aggravating blockage of, axonal flow.[7–9] Blood flow disturbance or alteration in deformed LC can diminish oxygen and nutrient supply and can accelerate RGC apoptosis.[8,10] Both the mechanical and ischemic mechanisms of LC deformation seem to be associated closely with glaucomatous change.

Lamina cribrosa deformation and its impact on glaucoma development and progression have been the focus of many in vivo studies. Lamina cribrosa deformation has been assessed mainly quantitatively for LC depth (LCD) in terms of its position relative to a reference plane. Glaucomatous eyes compared with healthy controls have shown LCD increase[11]; also, in primary open-angle glaucoma (POAG) eyes, LCD has been correlated positively with untreated intraocular pressure (IOP).[12] In LCD measurement, a common structural reference has been Bruch's membrane opening (BMO), especially for its demonstrably good interobserver reproducibility and agreement.[13,14] However, BMO location changes as a natural consequence of aging, specifically because of progressive choroidal thinning.[15] Thus, biased

assessment of LC location can result from applying the BMO as a reference point for LCD measurement.

Lamina cribrosa curvature could be a useful parameter for morphologic changes in LC because the LC curvature is not affected by choroidal thickness. Moreover, it may be hypothesized that the LC curvature index (LCCI), a simple index for LC posterior bowing, reflects the RGC axonal stress more accurately than does LCD.[16] Indeed, POAG eyes have shown greater LC curvature in comparison with healthy controls,[16] and LC curvature has been demonstrated to offer better glaucoma diagnostic performance than LCD.[17]

However, the relationship between the degree of LC posterior bowing and glaucoma progression has remained unclear. Therefore, the present longitudinal prospective study was undertaken to investigate the association between the degree of LC bowing and subsequent progression rates in POAG eyes.

Methods

This study was approved by the Seoul National University Hospital Institutional Review Board and adhered to the tenets of the Declaration of Helsinki. All participants provided written informed consent.

Study Participants

The participants of the current study comprised glaucoma patients from the Swept-Source Optical Coherence Tomography Study of Lamina Cribrosa, an ongoing prospective study at Seoul National University Hospital. To be included in the study, glaucoma patients were required to satisfy the definition of POAG, including the presence of glaucomatous optic disc changes such as diffuse or localized notching, or both; thinning; retinal nerve fiber layer (RNFL) defects on stereo disc photography, red-free fundus photography, or both; a glaucomatous visual field (VF) defect that corresponds to the structural change; and an open angle confirmed by gonioscopic examination. A glaucomatous VF defect was defined as (1) glaucoma hemifield test values outside the normal limits; (2) 3 or more abnormal contiguous points with a probability of $P < 0.05$, of which at least 1 point has a pattern deviation of $P < 0.01$; or (3) a pattern standard deviation of $P < 0.05$. The VF defects were confirmed on 2 consecutive reliable tests (fixation loss rate, $\leq 20\%$; false-positive and false-negative error rates, $\leq 25\%$).

All of the enrolled patients underwent a complete ophthalmic examination, including visual acuity assessment, refraction, slit-lamp biomicroscopy, Goldmann applanation tonometry (Haag-Streit, Koniz, Switzerland), dilated fundus examination, digital color stereo disc photography, red-free RNFL photography, central corneal thickness measurement (Orbscan 73 II; Bausch & Lomb Surgical, Rochester, NY), axial length (AL) measurement (Axis II PR; Quantel Medical, Inc., Bozeman, MT), and a central 30-2 threshold test of the Humphrey Visual Field (HFA II; Humphrey Instruments, Inc., Dublin, CA).

Because the purpose of the present study was to determine the rate of glaucomatous progression according to the baseline LC morphologic features, only early-stage glaucoma patients (initial VF mean deviation [MD], −5.0 to −0.01 dB)[18] were included in the subsequent analysis. For inclusion in the study, participants were required to have a best-corrected visual acuity of 20/40 or better in the Snellen equivalent and a spherical refraction of more than −6 diopters and less than +3 diopters.

Patients were excluded from further analysis for any of the following reasons: history of intraocular surgery (except uncomplicated cataract extraction) and any posterior pole lesions possibly affecting VF examination results. To assess the effect of baseline LC parameters on glaucoma progression clearly, only those patients with stable IOP during the entire follow-up were included selectively in the final analysis. That is, all patients included in the analysis received 1 or more topical glaucoma medications, and in all cases, the IOP was lowered by at least 20% from the untreated IOP and was maintained without any additional laser or surgical glaucoma interventions. Referred patients who had already used antiglaucoma medications also were excluded because it was impossible to assess IOP parameters accurately in such cases. If both eyes were qualified according to the inclusion criteria, 1 eye was selected randomly for further analysis.

Swept-Source OCT Imaging of Optic Disc

All eyes were scanned using a DRI OCT-1 Atlantis 3D swept-source (SS) OCT device (Topcon Medical Systems, Oakland, NJ) at 1 to 3 months after initiation of antiglaucoma medication. The baseline morphologic features of the LC were evaluated from 12 SS OCT radial line B-scans centered on the optic disc, with each scan at a half-clock-hour meridian. The final LC parameters (Fig 1) were calculated by averaging the values measured in the 12 directions over the full 360°, and the results were applied to the further analysis. All scans were reviewed to confirm if there was poor visualization of peripheral LC because of severe vascular shadowing or focal LC defects, and OCT scans with poor peripheral image quality were excluded from the further analysis. Also, eyes with more than 4 scans with poor peripheral LC visualization were excluded from the study. To enhance the visibility of the peripheral structure, adaptive compensation was applied to all of the scan images according to the previously published protocols.[19−21]

Measurement of Anterior Laminar Insertion Depth, Mean Lamina Cribrosa Depth, Mean Lamina Cribrosa Curvature Index, and Mean Adjusted Lamina Cribrosa Curvature Index

All of the measurements were performed by ImageJ software (National Institutes of Health, Bethesda, MD; available at http://image-j.nih.gov/ij/). For details on the measurement methods, the reader is referred to Fig 1 and a previously published article.[16] The anterior laminar insertion depth (ALID) was defined as the vertical distance between the anterior laminar insertion (ALI) and the reference plane connecting the BMO. The mean value of the 2 sides of the ALID was calculated as mean ALID for each plane. The area enclosed by the anterior laminar surface, the 2 vertical lines for the ALID measurement, and the BMO reference plane were measured. The LCD was computed by dividing this area by D (the length between the 2 cross-points made by vertical lines drawn from the ALI to the BMO reference plane). The anterior LC surface was drawn manually as if there were no discontinuity (e.g., vascular shadowing) on the anterior LC border. The LCD value was measured on each radial scan. The average LCD value over 360° was considered to be the final mean LCD (mLCD). The LCCI was defined as the difference between the LCD and the mean ALID (LCD minus mean ALID) on each scan. The average of all the LCCI measurements over 360° was defined as the final mean LCCI (mLCCI).

We also introduced a modified LCCI parameter, that is, the adjusted LCCI (aLCCI), to consider the steepness of the LC curve. Even with the same LCCI value, the smaller the length of D, the steeper the LC curve is. Therefore, the aLCCI was calculated as follows:

$$aLCCI = [LCCI / length D] \times 100.$$

The average aLCCI over 360° was defined as the final mean aLCCI (maLCCI). In 40 randomly selected eyes, all the parameters were
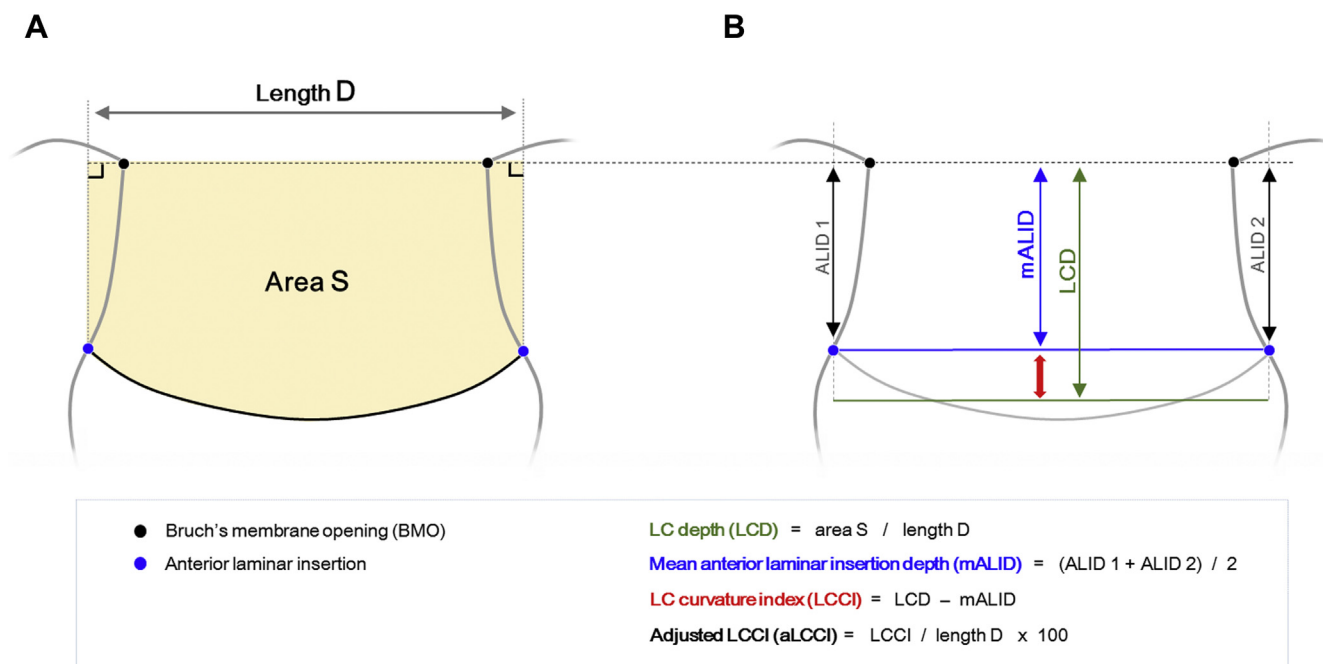
A

B

Figure 1. Diagrams showing measurement of lamina cribrosa (LC) parameters. **A**, Horizontal black dotted line connecting the 2 Bruch's membrane openings (BMOs) is selected as the reference plane, and the anterior lamina insertion (ALI) is depicted as blue dots. The 2 vertical lines were drawn from the ALI to the BMO reference plane, and the length between the 2 cross-points is defined as *D*. The area surrounded by the anterior LC surface, the 2 vertical lines, and the BMO reference line is defined as *S*, and the LCD is calculated by dividing *S* by *D*. **B**, Mean ALI depth (mALID) is the average value of the ALI depth on the 2 sides, and LC curvature index (LCCI) was defined as the difference between the LCD and mALID. The mALID, LCD, and LCCI are visualized by the blue, green, and red double-headed arrows, respectively. Even with the same LCCI value, the smaller the length *D*, the steeper the LC curve. To reflect the steepness of the LC curve, the adjusted LCCI (aLCCI) was computed by dividing LCCI by *D* and multiplying by 100.

measured independently by 2 experienced ophthalmologists (A.H. and T.J.K.) blinded to each patient's clinical information to evaluate the interobserver reproducibility of the measurements.

Measurement of Intraocular Pressure

A calibrated Goldmann applanation tonometer was used to measure untreated IOP (before initiation of topical medication) and at all follow-up visits thereafter. The mean IOP was calculated by averaging all the follow-up IOP values, and the percentage IOP reduction was computed based on the untreated and mean IOP values. Intraocular pressure fluctuation was defined as the standard deviation of the IOP at all visits starting at 1 month after initiation of medical treatment.

Visual Field Progression Assessment

The progression rate of VF defect was evaluated according to the MD slope of the Humphrey Field Analyzer. A linear regression analysis against time was performed to calculate the MD slope in each eye. The first 1 to 2 VF results were excluded to minimize the learning effects, and any unreliable results, as defined above, also were excluded. To be able to calculate a statistically significant MD slope, patients needed to have at least 5 reliable VF results (except the first 1 or 2 examinations) with a follow-up period of more than 3.5 years. Regarding the MD slope, eyes were classified as having progressed if there was a negative linear regression slope with a probability value of less than 0.05, and eyes that had an MD slope with a probability value 0.05 or more were excluded.

Data Analysis

The interobserver reproducibility of the mLCD, mLCCI, and maLCCI measurements was evaluated by calculating the intraclass correlation coefficients with their confidence intervals. A mixed-effect model was used to investigate how the rate of glaucoma progression (MD slope) was influenced by the mLCD, mLCCI, maLCCI, and other factors (age, gender, untreated IOP, percentage IOP reduction, mean IOP during follow-up, IOP fluctuation, refractive error, AL, central corneal thickness, occurrence of disc hemorrhage, baseline VF MD and pattern standard deviation, and total follow-up period), first with a univariate model and then with a multivariate model that included variables from the univariate model for which $P < 0.20$. Statistical analysis was performed using SAS software version 9.4 (SAS Institute, Inc., Cary, NC). A *P* value of less than 0.05 was considered statistically significant.

Results

Initially, 126 eyes meeting the eligibility criteria were enrolled. Among them, 18 were excluded because they had more than 4 OCT scans with poor image quality. Another 4 eyes were excluded because of associated retinal disease diagnosed over the course of the follow-up, and a further 3 eyes showing uncontrolled IOP also were excluded from the final analysis, leaving a final cohort of 101 eyes from 101 patients. Of 1212 scans from 101 eyes, 36 images were excluded because of poor image quality and 182 because of inability to localize the LC insertion point accurately, leaving 994 OCT scans available for analysis.

The participants' baseline mean age was 64.4±11.9 years (range, 40−86 years); among them, 53 were men (52.5%) and 48 were women (47.5%). The untreated IOP was 16.2±4.3 mmHg (range, 10−20.5 mmHg). The patients' clinical characteristics are summarized in Table 1.

Mean Lamina Cribrosa Depth, Mean Lamina Cribrosa Curvature Index, and Mean Adjusted Lamina Cribrosa Curvature Index

The mean baseline mLCD, mLCCI, and maLCCI were 419.0±111.2 μm (range, 180.0−734.2 μm), 76.4±29.0 μm (range, 15.3−158.7 μm), and 4.8±1.9 μm (range, 0.9−9.8 μm), respectively; none showed any statistically significant correlation with baseline VF MD ($P = 0.979$, $P = 0.439$, and $P = 0.327$, respectively). The interobserver intraclass correlation coefficients for the mLCD, mLCCI, and maLCCI measurements were 0.993, 0.968, and 0.989 (95% confidence intervals, 0.989−0.995, 0.953−0.978, and 0.983−0.992), respectively.

Rate of Visual Field Progression

The baseline MD was −3.8±3.4 dB (range, −5.0 to −0.01 dB) for the entire group of patients. After they were followed-up on for 3.6±0.8 years (range, 3.5−4.0 years), the mean MD slope was −0.18±0.33 dB/year (range, −2.01 to 0.17 dB/year). A total of 58 eyes (57.4%) showed a statistically significant negative MD slope, and among them, 22 eyes (21.7%) showed an MD progression rate of faster than −0.3 dB/year.

Determination of Factors Associated with Rate of Visual Field Progression

A univariate analysis revealed that a larger IOP fluctuation, a greater pattern standard deviation of baseline VF, a lower spherical equivalent, and greater baseline mLCD, mLCCI, and maLCCI were related to faster glaucomatous VF progression. In the

Table 1. Clinical Characteristics of Study Patients (n = 101)

Characteristics	Values
Age (yrs)	64.4±11.9
Gender (male/female)	53/48
Refractive error (D)	−1.4±3.0
Axial length (mm)	25.5±1.5
CCT (μm)	531.4±31.0
IOP (mmHg)	
Untreated IOP (mmHg)	16.2±4.3
Mean (mmHg)	13.2±1.4
At SS OCT scanning (mmHg)	12.4±2.3
Mean reduction (%)	23.4±14.6
Fluctuation (mmHg)	1.5±0.7
VF test	
Baseline MD (dB)	−3.8±3.4
Baseline PSD (dB)	5.1±3.8
No. of examinations	7.2±1.5
Follow-up	
Total (yrs)	3.6±0.8
Mean interval (mos)	6.2±0.3

CCT = central corneal thickness; D = diopters; IOP = intraocular pressure; MD = mean deviation; PSD = pattern standard deviation; SS = swept-source; VF = visual field.
Values are mean ± standard deviation.

multivariate analysis, considering the multicollinearity of the LC parameters, the final optimal model was selected by a stepwise model selection method based on the Akaike information criterion index and Bayesian information criterion. According to the final model selected, the rate of VF MD deterioration was associated significantly with the baseline maLCCI value adjusting for IOP fluctuation, VF pattern standard deviation, and spherical equivalent ($P < 0.001$; Tables 2 and 3).

Assessment of Relationship between Mean Adjusted Lamina Cribrosa Curvature Index and Rate of Visual Field Progression

In a scattergram, the relationship between the maLCCI and the rate of VF progression was expected to have a certain maLCCI point at which the MD slope significantly represents a negative value. To estimate the optimal cutoff value, the model was fitted after excluding the upper and lower 5% results. The best-fitting continuous segmented model of the relationship between the maLCCI and the rate of MD progression was formulated as:

$$Y = \beta_0 + \beta_2 X,$$
$$X = 0, \text{ if } x < c \text{ and } X = x - c, \text{ otherwise,}$$

where Y is the MD slope in decibels per year, X is the maLCCI, and c is the optimal cutoff point. This analysis identified 4.12 as the significant breakpoint ($R^2 = 0.72$; $P < 0.001$; Fig 2A). If the maLCCI was greater than the breakpoint (4.12), the rate of VF progression (i.e., MD slope) increased by −0.02 dB/year as the maLCCI increased by 0.1 unit.

Investigation of Age-Dependent Difference in Association between Mean Adjusted Lamina Cribrosa Curvature Index and Rate of Visual Field Progression

The correlation between the maLCCI and the MD slope was analyzed according to patient age. The age cutoff for this analysis was obtained by the minimum P value approach (available at http://www.mayo.edu/research/documents/biostat-79pdf/doc-10027230) using a 2-fold validation method. This statistical analysis revealed that the age of 69 years best explained the difference in the relationship between the maLCCI and VF progression in our study participants. The rate of MD deterioration was accelerated by −0.014 dB/year ($R^2 = 0.64$; $P < 0.001$) and −0.006 dB/year ($R^2 = 0.58$; $P = 0.017$) per 1-unit increase in maLCCI in the younger and older age groups, respectively. According to the 2-fold cross-validation method, a significant difference in the correlation between the maLCCI and MD slope based on the obtained cutoff age was confirmed ($P = 0.043$; Fig 2B).

Representative Cases

Figure 3 shows representative cases of a greater maLCCI with faster VF progression and a smaller maLCCI with a stable VF MD. The first and second rows in the figure are the findings for a man 56 years of age at the time of SS OCT who demonstrated an maLCCI of 8.70 and an MD slope of −0.65 dB/year. His untreated IOP was 14.0 mmHg and his mean IOP during follow-up was 11.1 mmHg. The IOP fluctuation was calculated as 1.7 mmHg. The third and fourth rows in the figure are the results for a man 44 years of age at the time of SS OCT who demonstrated an maLCCI of 3.34 and an MD slope of −0.06 dB/year. His untreated IOP, mean IOP, and IOP fluctuation values were 18.0 mmHg, 14.2 mmHg, and 1.7 mmHg, respectively.

Table 2. Factors Associated with Glaucomatous Visual Field Progression

	Univariate Analysis				Multivariate Analysis			
	Estimate	Standard Error	95% Confidence Interval	P Value	Estimate	Standard Error	95% Confidence Interval	P Value
Age (yrs)	< 0.001	0.005	−0.009 to 0.009	0.99				
Gender (male)	0.061	0.105	−0.153 to 0.274	0.57				
Untreated IOP (mmHg)	−0.013	0.022	−0.057 to 0.030	0.54				
Mean IOP reduction (%)	0.009	0.013	−0.004 to 0.015	0.75				
Mean IOP (mmHg)	−0.034	0.040	−0.015 to 0.007	0.32				
IOP fluctuation (mmHg)	**−0.039**	**0.022**	**−0.083 to 0.004**	**0.07**	−0.009	0.014	−0.037 to 0.019	0.52
Refractive error (D)	**0.041**	**0.018**	**0.006 to 0.077**	**0.02**	0.003	0.012	−0.022 to 0.027	0.82
Axial length (mm)	0.005	0.013	−0.020 to 0.048	0.58				
CCT (μm)	−0.001	0.002	−0.004 to 0.003	0.92				
History of disc hemorrhage	−0.164	0.137	−0.442 to 0.115	0.24				
Baseline VF MD (dB)	0.007	0.015	−0.022 to 0.036	0.63				
Baseline VF PSD (dB)	**−0.022**	**0.013**	**−0.048 to −0.003**	**0.09**	−0.001	0.008	−0.017 to 0.017	0.97
Mean LCD (μm)	**−0.001**	**0.001**	**−0.002 to −0.001**	**0.01**				
Mean LCCI (μm)	**−0.012**	**0.001**	**−0.015 to −0.010**	**<0.001**				
Mean aLCCI	**−0.193**	**0.016**	**−0.225 to −0.161**	**<0.001**	**−0.190**	**0.017**	**−0.225 to −0.155**	**<0.001**
Total follow-up (mos)	0.013	0.040	−0.070 to 0.080	0.68				

aLCCI = adjusted lamina cribrosa curvature index; CCT = central corneal thickness; D = diopters; IOP = intraocular pressure; LCCI = lamina cribrosa curvature index; LCD = lamina cribrosa depth; MD = mean deviation; PSD = pattern standard deviation; VF = visual field.
All values <0.2 at univariate analysis and <0.05 at multivariate analysis are presented in boldface.

Discussion

This study demonstrated the association of a greater baseline maLCCI with a significantly faster subsequent VF progression rate in POAG eyes. Additionally, we found a statistically significant maLCCI breakpoint above which there was a greater MD slope.

Both LCD and the LCCI have been used to evaluate the degree of LC posterior deformation as an indication of LC morphologic features. The LCD heretofore has been measured mostly from the reference plane BMO to the anterior LC surface.[11,13] However, this methodology inevitably includes choroidal thickness in the determined LCD value, which can incur bias in LC morphologic assessment. Alternatively, the LCCI could reflect the degree of LC deformation more accurately for 2 reasons: the LCCI is robust to the effect of choroidal thickness and posterior bowing of the LC is evaluated from the insertion point. Further, the newly introduced parameter, aLCCI, can reflect the degree of steepness of the LC curve. Our findings in the present study suggest that the aLCCI is a better LC deformation and RGC axonal stress parameter.

The degree of posterior LC bowing would be determined by the load-bearing LC tissue's mechanical response to stress in addition to the amounts of IOP-induced stress and strain.[22] That is, the degree of LC deformation, for a given IOP and cerebrospinal fluid pressure, is a function of the mechanical properties of the LC tissue. Ex vivo or nonhuman primate studies have shown that with age, collagen content as well as LC thickness changes,[23,24] and the LC's mechanical compliance is known to decrease with age.[24,25] The LC in older eyes tends to be shallower than that in younger eyes at a given VF defect level.[25] Additionally, an association has been found between younger age and a larger LC curvature decrement after postoperative IOP reduction.[26] Lee et al[27]

showed that faster RNFL thinning is related to greater LCD only in younger (age <63 years) patients. Thus, it is reasonable to hypothesize that the relationship between LC characteristics and further glaucomatous damage may be affected by patient age.

Indeed, in the current study, the relationship of the maLCCI to the VF progression rate varied with age. Specifically, progression of VF was more accelerated per unit change in maLCCI in the relatively younger age group (age ≤69 years) than in the older group. We can speculate that the more pliant LC microstructure of younger individuals potentially causes more kinking and pinching of the axons in the laminar pores, even for a similar degree of curvature change, thus inducing faster glaucomatous deterioration. Also, there remains the possibility that various factors other than LC deformation have more impact in older glaucoma patients.

Lamina cribrosa deformation has been noted to occur mostly in the early stages of glaucoma. Park et al[28] showed that LCD was the deepest in mild to moderate glaucoma

Table 3. The Results of Model Selection Criterion

Variables in the Model	Akaike Information Criterion	Bayesian Information Criterion
mLCD, mLCCI, maLCCI	98.4	102.7
mLCD, mLCCI	101.8	106.1
mLCD, maLCCI	90.4	94.7
mLCCI, maLCCI	84.2	88.5
mLCD	158.3	162.6
mLCCI	87.7	92.0
maLCCI	76.3	80.6

maLCCI = mean adjusted lamina cribrosa curvature index; mLCCI = mean lamina cribrosa curvature index; mLCD = mean lamina cribrosa depth.
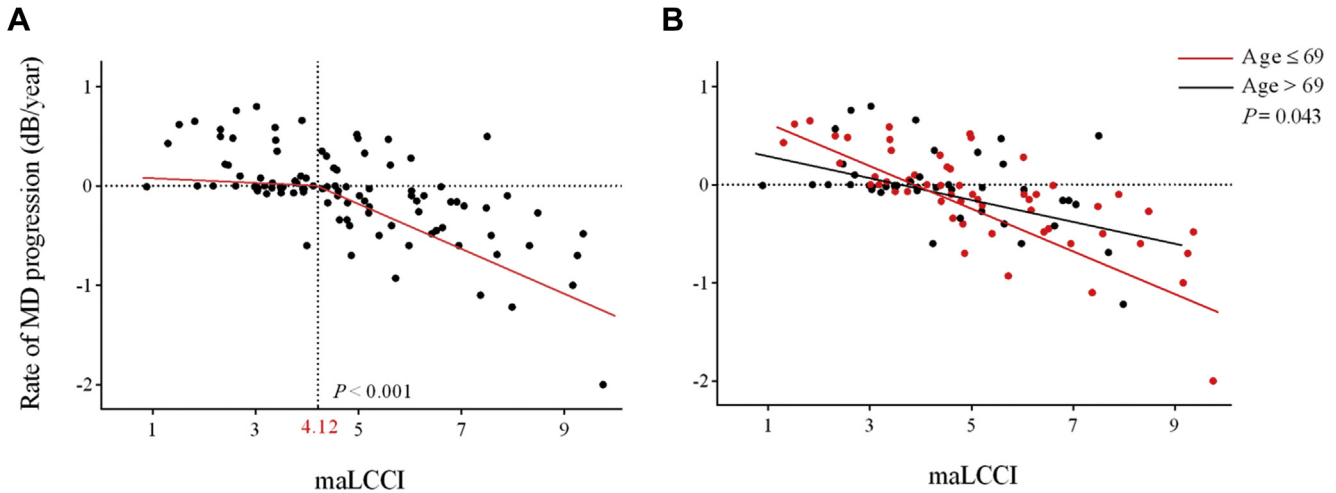
A

B

Figure 2. A, Scatterplot showing the significant breakpoint of the mean adjusted lamina cribrosa curvature index (maLCCI) after which the mean deviation (MD) slope becomes steeper. Note that the slope changes at the point where the maLCCI exceeds 4.12 (*P* < 0.001). **B,** Scatterplot showing age-related differences in relationship between baseline maLCCI and visual field MD slope. Note that as the maLCCI changes by 1 unit, MD progression is faster in the younger age group (age ≤69 years; *P* = 0.043).

followed by preperimetric glaucoma and, finally, healthy eyes. However, the same study found no significant difference between eyes with mild to moderate glaucoma and those with severe glaucoma. Additionally, previous studies conducted on experimental early glaucoma monkeys revealed that LC from the onset of glaucoma not only deforms, but also remodels, in response to its altered biomechanical environment.[29,30] In the present study, eyes with a significantly faster rate of VF progression manifested greater LC deformation from the early disease stage. This indicates that the LC morphologic changes in early-stage glaucoma potentially lead to the greater vulnerability of RGC axons to subsequent disease progression. That is, with greater posterior bowing of the LC, RGC axons increasingly are susceptible to further glaucomatous injury; as such, the maLCCI could serve as a particularly valuable early indicator of subsequent functional progression in POAG.

The LC in healthy eyes typically has a saddle-like configuration. Thus, LC parameters would be expected to show topographic variation. Kim et al[31] demonstrated that in normal-tension glaucoma eyes, the vertical-to-horizontal ALID difference was greater than that in normal eyes, and that in high-tension glaucoma patients, the horizontal ALI was located more posteriorly and the laminar curvature was much increased, resulting in a U-shaped rather than W-shaped LC contour. These results indicate that LC topographic variation can be much greater and can vary more widely in glaucomatous eyes. In previous studies, the LC has been evaluated mainly in 2 meridians: horizontal and vertical. In the present study, we used LC parameter measurements averaged over 360° to reflect best the topographic variation in different directions. Despite this strength of the present study, we believe that more detailed planar–structural evaluation of LC morphologic features is needed to assess more accurately the LC deformation in a 3-dimensional perspective.

None of the IOP-related factors were associated significantly with the rate of VF progression in our study. This contradicts the results of previous studies indicating that IOP and its related parameters are important glaucoma progression risk factors.[32,33] This discrepancy may have resulted from the relatively low pretreatment and posttreatment IOP levels in our study group (16.2±4.3 mmHg and 13.2±1.4 mmHg, respectively). In the present study, only patients in whom IOP remained stable during the entire follow-up period were included, and this could be another relevant factor. We applied more intense IOP-lowering treatment to progressing eyes, which also could have incurred a bias in the relationship between the IOP parameters and the rate of glaucomatous VF progression. In addition, it is possible that our study did not investigate various parameters sufficiently that are associated with IOP.

The present study's findings must be interpreted in the light of its limitations. First, the LC structure was not evaluated at the earliest stage of glaucomatous change, because LC deformation has been found to start even before RNFL thinning.[34–36] Especially because the LC's connective tissue structure can be altered over time, the LC morphologic features that manifest before initial glaucomatous change may provide a more accurate reflection of further disease progression. Second, localization of LC insertion point and delineation of the anterior surface of the LC can be highly subjective. The visibility of the ALI has been much improved by newly developed OCT devices and adaptive compensation algorithms, but manual calculations, as used in the present study, especially for the ALI point, inevitably have less histologic support. Also, this study included only patients with early stage glaucoma, making visualization of ALI even more difficult. Therefore, the possibility of errors in detection of the ALI and delineation of the surface of the LC should be considered when interpreting the results of this study. Third, adjustment of the magnification effect according to
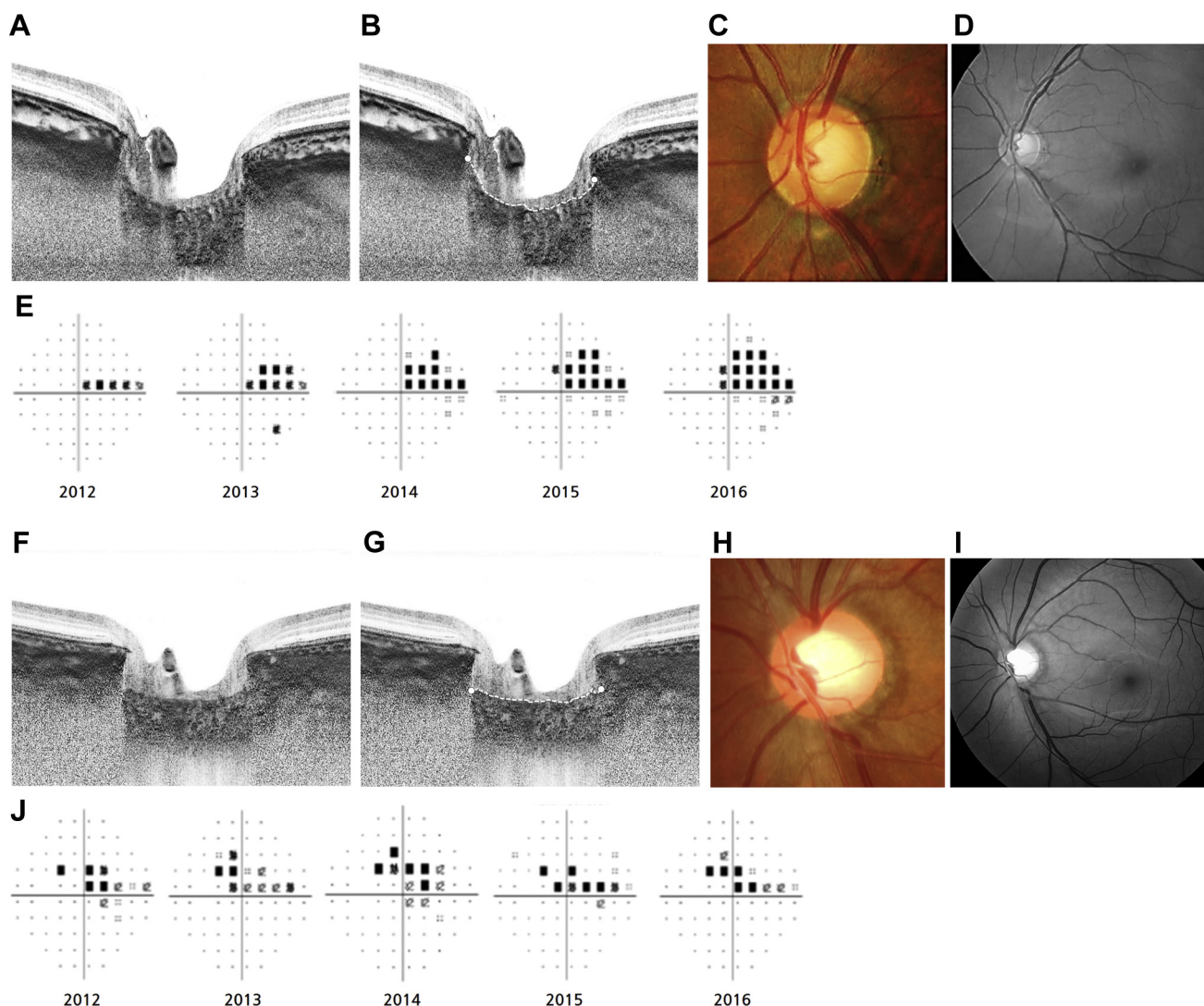
Figure 3. Images form representative patients showing the relationship between the mean adjusted lamina cribrosa curvature index (maLCCI) at baseline and subsequent visual field (VF) progression. Horizontal swept-source (SS) OCT optic disc B-scans of eyes with (**A**, **B**) a greater and (**F**, **G**) a smaller maLCCI. The image delineated with guidelines is the same as that depicted to the left, and the anterior surface of the lamina cribrosa has been depicted manually as a white dotted line. The first and third rows contain stereo disc photographs and red-free retinal nerve fiber layer (RNFL) photographs in eyes with (**C**, **D**) greater and (**H**, **I**) smaller maLCCI. The stereo disc photographs and RNFL photographs were performed on the same dates as the SS OCT scans. The second and fourth rows show the results of Humphrey VF C30-2 pattern deviation plots for eyes with (**E**) greater and (**J**) smaller maLCCI.

interindividual differences in AL was not performed in this study. According to Littman,[37] the uncorrected lateral measurement is decreased with increasing AL, which could affect the results of LC measurements. However, in the current study, the AL was distributed within a relatively narrow range (22.55−25.40 mm). Furthermore, we estimated the maximum effect of magnification error on maLCCI measurement by comparing the values with and without AL adjustment in the longest and the shortest AL in our study participants, and the measurement error was less than 13%. Therefore, we cautiously estimated that the difference in AL would not have had a critical impact on our results. Nevertheless, the effects of a difference in AL on the measurement obtained for each LC parameter should be investigated in future studies. Fourth, all enrolled

participants were POAG patients with untreated IOP of 21 mmHg or less. Lamina cribrosa morphologic features can alter as IOP changes.[26,38] Therefore, our results may not be applicable directly to POAG patients showing higher baseline IOP who demonstrate a greater IOP reduction rate after treatment. Fifth, the average 3.6-year follow-up period can be considered to be too short for evaluation of the LC deformation's long-term effects on glaucoma progression. Further studies should investigate the influences of LC characteristics on longer-term disease prognosis.

In conclusion, this study found a significant correlation between the baseline maLCCI and subsequent VF progression rate in eyes with POAG. This suggests that with greater posterior bowing of the LC, RGC axons increasingly are vulnerable to further glaucomatous injury. Therefore,

baseline LC characteristics could serve as supplementary prognostic factors in further glaucoma progression. Eyes showing greater LC deformation should be monitored more carefully while keeping the possibility of VF deterioration in mind.

References

1. Quigley HA, Addicks EM. Regional differences in the structure of the lamina cribrosa and their relation to glaucomatous optic nerve damage. *Arch Ophthalmol*. 1981;99(1):137−143.
2. Radius RL, Gonzales M. Anatomy of the lamina cribrosa in human eyes. *Arch Ophthalmol*. 1981;99(12):2159−2162.
3. Quigley HA, Addicks EM, Green WR, Maumenee AE. Optic nerve damage in human glaucoma. II. The site of injury and susceptibility to damage. *Arch Ophthalmol*. 1981;99(4):635−649.
4. Quigley H, Anderson DR. The dynamics and location of axonal transport blockade by acute intraocular pressure elevation in primate optic nerve. *Invest Ophthalmol Vis Sci*. 1976;15(8):606−616.
5. Quigley H, Anderson DR. Distribution of axonal transport blockade by acute intraocular pressure elevation in the primate optic nerve head. *Invest Ophthalmol Vis Sci*. 1977;16(7):640−644.
6. Gaasterland D, Tanishima T, Kuwabara T. Axoplasmic flow during chronic experimental glaucoma. 1. Light and electron microscopic studies of the monkey optic nervehead during development of glaucomatous cupping. *Invest Ophthalmol Vis Sci*. 1978;17(9):838−846.
7. Yang H, Downs JC, Girkin C, et al. 3-D histomorphometry of the normal and early glaucomatous monkey optic nerve head: lamina cribrosa and peripapillary scleral position and thickness. *Invest Ophthalmol Vis Sci*. 2007;48(10):4597−4607.
8. Burgoyne CF, Downs JC, Bellezza AJ, et al. The optic nerve head as a biomechanical structure: a new paradigm for understanding the role of IOP-related stress and strain in the pathophysiology of glaucomatous optic nerve head damage. *Prog Retin Eye Res*. 2005;24(1):39−73.
9. Burgoyne CF, Morrison JC. The anatomy and pathophysiology of the optic nerve head in glaucoma. *J Glaucoma*. 2001;10(5):S16−S18.
10. Roberts MD, Sigal IA, Liang Y, et al. Changes in the biomechanical response of the optic nerve head in early experimental glaucoma. *Invest Ophthalmol Vis Sci*. 2010;51(11):5675−5684.
11. Furlanetto RL, Park SC, Damle UJ, et al. Posterior displacement of the lamina cribrosa in glaucoma: in vivo interindividual and intereye comparisons. *Invest Ophthalmol Vis Sci*. 2013;54(7):4836−4842.
12. Jung KI, Jung Y, Park KT, Park CK. Factors affecting plastic lamina cribrosa displacement in glaucoma patients: factors affecting LC depth in glaucoma. *Invest Ophthalmol Vis Sci*. 2014;55(12):7709−7715.
13. Park SC, Kiumehr S, Teng CC, et al. Horizontal central ridge of the lamina cribrosa and regional differences in laminar insertion in healthy subjects. *Invest Ophthalmol Vis Sci*. 2012;53(3):1610−1616.
14. Agoumi Y, Sharpe GP, Hutchison DM, et al. Laminar and prelaminar tissue displacement during intraocular pressure elevation in glaucoma patients and healthy controls. *Ophthalmology*. 2011;118(1):52−59.
15. Johnstone J, Fazio M, Rojananuangnit K, et al. Variation of the axial location of Bruch's membrane opening with age, choroidal thickness, and race. *Invest Ophthalmol Vis Sci*. 2014;55(3):2004−2009.
16. Kim YW, Jeoung JW, Girard MJ, et al. Clinical assessment of lamina cribrosa curvature in eyes with primary open-angle glaucoma. *PLoS One*. 2016;11(3), e0150260.
17. Lee SH, Kim T-W, Lee EJ, et al. Diagnostic power of lamina cribrosa depth and curvature in glaucoma: diagnostic power of LC depth and curvature. *Invest Ophthalmol Vis Sci*. 2017;58(2):755−762.
18. Mills RP, Budenz DL, Lee PP, et al. Categorizing the stage of glaucoma from pre-diagnosis to end-stage disease. *Am J Ophthalmol*. 2006;141(1):24−30.
19. Girard MJ, Tun TA, Husain R, et al. Lamina cribrosa visibility using optical coherence tomography: comparison of devices and effects of image enhancement techniques. Lamina cribrosa visibility in OCT. *Invest Ophthalmol Vis Sci*. 2015;56(2):865−874.
20. Girard MJ, Strouthidis NG, Ethier CR, Mari JM. Shadow removal and contrast enhancement in optical coherence tomography images of the human optic nerve head. *Invest Ophthalmol Vis Sci*. 2011;52(10):7738−7748.
21. Strouthidis N, Mari JM, Park SC, Girard M. Enhancement of lamina cribrosa visibility in optical coherence tomography images using adaptive compensation. *Invest Ophthalmol Vis Sci*. 2013;54(15), 2149−2149.
22. Morgan WH, Chauhan BC, Yu D-Y, et al. Optic disc movement with variations in intraocular and cerebrospinal fluid pressure. *Invest Ophthalmol Vis Sci*. 2002;43(10):3236−3242.
23. Albon J, Karwatowski W, Avery N, et al. Changes in the collagenous matrix of the aging human lamina cribrosa. *Br J Ophthalmol*. 1995;79(4):368−375.
24. Kotecha A, Izadi S, Jeffery G. Age-related changes in the thickness of the human lamina cribrosa. *Br J Ophthalmol*. 2006;90(12):1531−1534.
25. Ren R, Yang H, Gardiner SK, et al. Anterior lamina cribrosa surface depth, age, and visual field sensitivity in the Portland Progression Project: laminar depth and age in glaucoma. *Invest Ophthalmol Vis Sci*. 2014;55(3):1531−1539.
26. Lee EJ, Kim T-W, Weinreb RN. Reversal of lamina cribrosa displacement and thickness after trabeculectomy in glaucoma. *Ophthalmology*. 2012;119(7):1359−1366.
27. Lee EJ, Kim T-W, Kim M, Kim H. Influence of lamina cribrosa thickness and depth on the rate of progressive retinal nerve fiber layer thinning. *Ophthalmology*. 2015;122(4):721−729.
28. Park SC, Brumm J, Furlanetto RL, et al. Lamina cribrosa depth in different stages of glaucoma. *Invest Ophthalmol Vis Sci*. 2015;56(3):2059−2064.
29. Downs JC, Roberts MD, Sigal IA. Glaucomatous cupping of the lamina cribrosa: a review of the evidence for active progressive remodeling as a mechanism. *Exp Eye Res*. 2011;93(2):133−140.
30. Roberts MD, Grau V, Grimm J, et al. Remodeling of the connective tissue microarchitecture of the lamina cribrosa in early experimental glaucoma. *Invest Ophthalmol Vis Sci*. 2009;50(2):681−690.
31. Kim YW, Jeoung JW, Girard MJ, et al. Positional and curvature difference of lamina cribrosa according to the baseline intraocular pressure in primary open-angle glaucoma: a swept-source optical coherence tomography (SS-OCT) study. *PLoS One*. 2016;11(9), e0162182.
32. Group CN-TGS. The effectiveness of intraocular pressure reduction in the treatment of normal-tension glaucoma. *Am J Ophthalmol*. 1998;126(4):498−505.
33. Leske MC, Heijl A, Hussein M, et al. Factors for glaucoma progression and the effect of treatment: the Early Manifest Glaucoma Trial. *Arch Ophthalmol*. 2003;121(1):48−56.
34. Xu G, Weinreb RN, Leung CK. Optic nerve head deformation in glaucoma: the temporal relationship between optic nerve

head surface depression and retinal nerve fiber layer thinning. *Ophthalmology*. 2014;121(12):2362−2370.

35. He L, Yang H, Gardiner SK, et al. Longitudinal detection of optic nerve head changes by spectral domain optical coherence tomography in early experimental glaucoma: detection of ONH changes by SDOCT in glaucoma. *Invest Ophthalmol Vis Sci*. 2014;55(1):574−586.

36. Strouthidis NG, Fortune B, Yang H, et al. Longitudinal change detected by spectral domain optical coherence tomography in the optic nerve head and peripapillary retina in experimental glaucoma. *Invest Ophthalmol Vis Sci*. 2011;52(3):1206−1219.

37. Littmann H. [Determination of the real size of an object on the fundus of the living eye]. *Klin Monbl Augenheilkd*. 1982;180(4):286−289.

38. Wu Z, Xu G, Weinreb RN, et al. Optic nerve head deformation in glaucoma: a prospective analysis of optic nerve head surface and lamina cribrosa surface displacement. *Ophthalmology*. 2015;122(7):1317−1329.

Footnotes and Financial Disclosures

[1] Department of Ophthalmology, Seoul National University College of Medicine, Seoul, Republic of Korea.

[2] Department of Ophthalmology, Seoul National University Hospital, Seoul, Republic of Korea.

[3] Department of Biomedical Engineering, National University of Singapore, Singapore, Republic of Singapore.

[4] Singapore Eye Research Institute and Singapore National Eye Centre, Singapore, Republic of Singapore.

[5] Science Technology and Health Department, University of French Polynesia, Tahiti, French Polynesia.

Abbreviations and Acronyms:

AL = axial length; **aLCCI** = adjusted lamina cribrosa curvature index; **ALI** = anterior laminar insertion; **ALID** = anterior laminar insertion depth; **BMO** = Bruch's membrane opening; **D** = distance between the 2 cross-points made by vertical lines drawn from the anterior laminar insertion to the reference plane of Bruch's membrane opening; **IOP** = intraocular pressure; **LC** = lamina cribrosa; **LCD** = lamina cribrosa depth; **LCCI** = lamina cribrosa curvature index; **maLCCI** = mean adjusted lamina cribrosa curvature index; **MD** = mean deviation; **mLCCI** = mean lamina cribrosa curvature index; **mLCD** = mean lamina cribrosa depth; **POAG** = primary open-angle glaucoma; **RGC** = retinal ganglion cell; **RNFL** = retinal nerve fiber layer; **SS** = swept-source; **VF** = visual field.

Correspondence:

Jin Wook Jeoung, MD, PhD, Department of Ophthalmology, Seoul National University Hospital, Seoul National University College of Medicine, 101 Daehak-ro, Chongno-gu, Seoul, Republic of Korea. E-mail: neuroprotect@gmail.com.